Computational Materials Science 176 (2020) 109520

Contents lists available at ScienceDirect

Computational Materials Science

journal homepage: www.elsevier.com/locate/commatsci

Structural optimization and melting behavior investigation of Pd-Ag bimetallic nanoparticles by molecular simulations

Mingming Guo[a], Huizhen He[a], Zhipeng Zhang[a], Zhitian Liu[a], Feng Xie[b], Bin Shan[c,*], Xianbao Duan[a,b,*]

[a] Institute of Materials for Optoelectronics and New Energy, School of Materials Science and Engineering, Wuhan Institute of Technology, Wuhan 430205, Hubei, People's Republic of China

[b] Institute of Nuclear and New Energy Technology, Collaborative Innovation Center of Advanced Nuclear Energy Technology, Key Laboratory of Advanced Reactor Engineering and Safety of Ministry of Education, Tsinghua, Beijing 100084, People's Republic of China

[c] School of Materials Science and Engineering, Huazhong University of Science and Technology, Wuhan 430074, Hubei, People's Republic of China

ARTICLE INFO

Keywords:
Pd-Ag nanoparticle
Molecular simulation
Genetic algorithm
Melting behavior

ABSTRACT

Pd-Ag bimetallic nanoparticles have been researched among many fields due to their excellent electronic, catalytic and optical properties. It's of great significance to learn about the corresponding structural characteristics with respect to the shape, the composition and the size from atomic scale. In present work, improved genetic algorithm accompanied by molecular statics simulations is applied to investigate the structural stability of Pd-Ag nanoparticles systematically. Specifically, the atomic arrangements of eight typical shaped Pd-Ag nanoparticles with different compositions and sizes are studied. Indicators based on energetics are used to characterize the structural stability. It has shown that the Pd-Ag nanoparticles with icosahedral shape are the most stable. Besides, the melting behavior of Pd-Ag nanoparticles is explored using molecular dynamics simulations and Lindemann index is employed to indicate the melting point. It is found that the melting points increase as the size increases and the icosahedral shape of Pd-Ag nanoparticles have the highest melting points.

1. Introduction

In the past decades, nanoparticles (NPs) have been extensively investigated due to their excellent electronic, catalytic and optical properties [1–3]. In the catalytic field, bimetallic NPs have shown much better performance compared to monometallic NPs [4,5]. The unique bimetallic synergetic effect, which derives from the change of electronic structure due to the coordinated unsaturated atoms after alloying, has also been theoretically confirmed [6]. As the structures of NPs determine the corresponding physical and chemical properties intrinsically, it is of great significance to understand the structural characteristics of bimetallic NPs from atomic scale.

As a typical bimetallic NP, the Pd-Ag system is of great interest in the application of catalysis due to its special performance, such as enhancing the selectivity in hydrogenation reactions [7,8]. It has been demonstrated that the addition of Ag to the Pd NPs can significantly reduce surface hydrogen much more than subsurface hydrogen [9]. Compared to the commercial Pd-C catalyst, the catalyst composed of Pd-Ag bimetallic NPs exhibits superior electrocatalytic activity and stability towards ethanol electro-oxidation in alkaline media [10]. Hence, as a new non-Pt electro-catalyst, Pd-Ag NP is with great potential for direct alcohol fuel cells [11]. As is well-known, the catalytic performance of Pd-Ag NPs is strongly dependent on the structural characteristics, such as the shape, the composition, the size and so on [12]. Hence, it's particularly meaningful to investigate the structural characteristics of Pd-Ag bimetallic NPs.

In present work, the structural characteristics of Pd-Ag bimetallic NPs with different shapes, compositions and sizes are studied using improved genetic algorithm accompanied by molecular statics simulations systematically. Besides, the melting behavior of all involved Pd-Ag NPs are researched using molecular dynamics (MD) simulations. The paper is organized as the following: Section 2 is an introduction to the methods used in present work, Section 3 presents the obtained results and corresponding discussions, and Section 4 is a short summary on the main conclusions.

* Corresponding authors.
E-mail addresses: bshan@mail.hust.edu.cn (B. Shan), xianbao.d@gmail.com, xbduan@wit.edu.cn (X. Duan).

https://doi.org/10.1016/j.commatsci.2020.109520
Received 22 October 2019; Received in revised form 1 January 2020; Accepted 6 January 2020
Available online 21 January 2020
0927-0256/

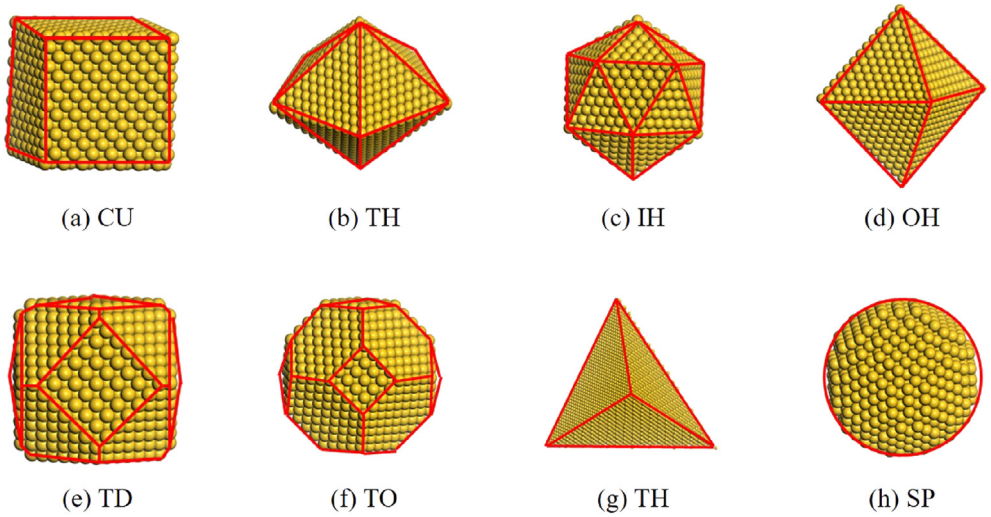

Fig. 1. Schematic models of the eight involved shapes of Pd-Ag NPs in present work: (a) cube (CU); (b) decahedron (DH); (c) icosahedrons (IH); (d) octahedron (OH); (e) tetrakaidecahedron (TD); (f) truncated octahedron (TO); (g) tetrahedron (TH); (h) sphere (SP).

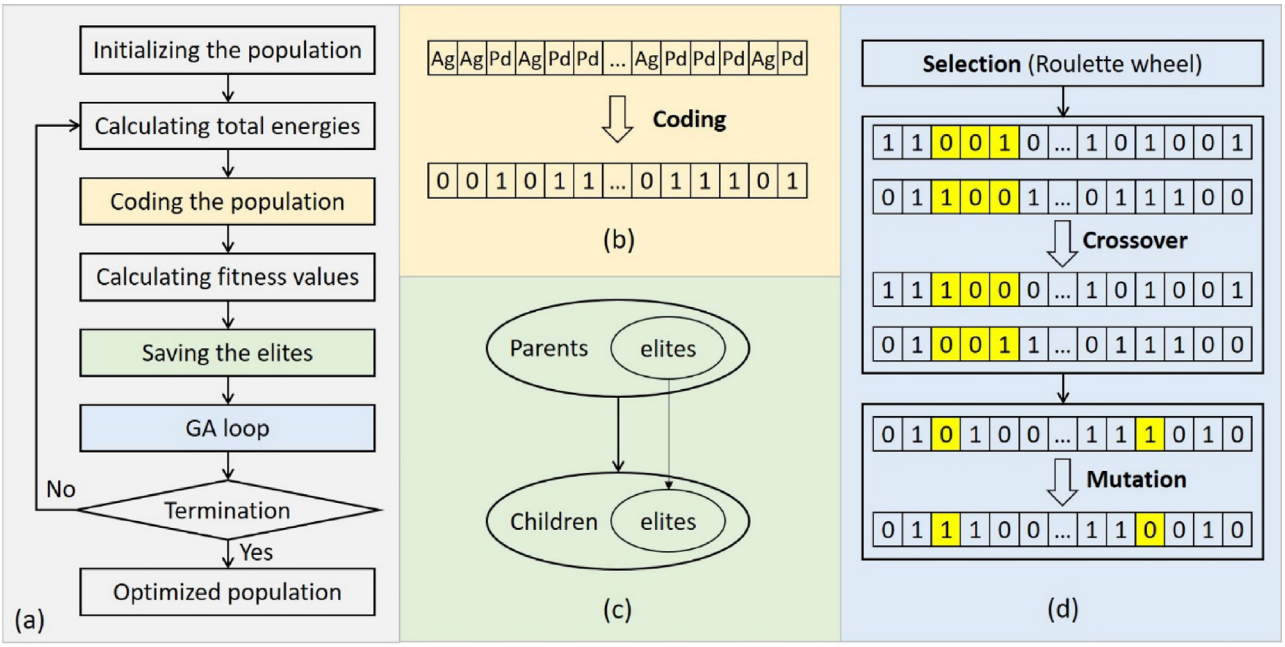

Fig. 2. Schematic diagram of the improved genetic algorithm to optimize the atomic arrangement of Pd-Ag NP. (a) is the flowchart of the GA process, (b), (c) and (d) are diagrams for coding the population, saving the elites and GA loop (including selection, crossover and mutation), respectively.

2. Methodology

2.1. Model construction

Pd-Ag bimetallic NPs can be presented with different shapes, such as core-shell, ordered or random structures, which depends on the preparation methods [9]. In present work, seven typical polyhedral shapes of Pd-Ag NPs are constructed, as: (1) cube (CU), enclosed by six {1 0 0} facets; (2) decahedron (DH), enclosed by ten {1 1 1} facets; (3) icosahedrons (IH), enclosed by twenty {1 1 1} facets; (4) octahedron (OH), enclosed by eight {1 1 1} facets; (5) tetrakaidecahedron (TD), enclosed by six {1 0 0} facets; (6) truncated octahedron (TO), enclosed by eight {1 1 1} facets; (7) tetrahedron (TH), enclosed by four {1 1 1} facets. Besides, spherical (SP) shape of Pd-Ag NPs is also constructed as a comparison. Fig. 1 shows the schematic models of the eight involved shapes.

Apart from the shape, the effects of composition and size on the structural characteristics of Pd-Ag NPs are also investigated in present work. Hence, the NPs with different compositions and sizes are also constructed. Details on the construction of a specific Pd-Ag NP can be described as follows. Firstly, a three-dimensional crystal structure, which is slightly larger than the final NP, is constructed. During the construction, face-centered cubic (FCC), which is the ground state structure for both Pd and Ag, is adopted as the basic framework of lattice points. The lattice constant is set using Vegard's law according to the composition ratio of Ag/Pd in the NP. Then the initial NP can be obtained by cutting the three-dimensional crystal structure based on specified shape and size. Finally, the lattice points of the initial NP are filled with Pd atoms and Ag atoms randomly according to the composition ratio.

2.2. Improved genetic algorithm

To explore the structural characteristics of Pd-Ag NPs, the atomic

arrangement with the lowest energy should be found from the huge search space consisting of different atomic arrangements firstly. Essentially, it is a global optimization problem. Although there is no available algorithm which can solve such problems theoretically, some effective algorithms have been developed for practical applications in the past years, such as Monte Carlo, simulated annealing, particle swarm optimization and genetic algorithm [13–17]. In present work, genetic algorithm (GA) is employed to optimize atomic arrangement of specified Pd-Ag NP. To enhance the efficiency of the optimization process, the classical GA has been improved by incorporating some modifications. Fig. 2 gives the scheme of the improved GA used in present work and Fig. 2(a) shows the flowchart of the improved GA process, which mainly consists of the following seven steps.

To facilitate the introduction of the improved genetic algorithm used in present work, a brief explanation of several basic concepts are given firstly. *Population* and *individual* are two basic concepts in GA. In present work, an *individual* corresponds to a Pd-Ag NP with specific atomic arrangement. A *population*, which can be regarded as a *generation* from the view of evolution, is a collection of different individuals. Since individuals in the same population are usually different from each other, *chromosome*, composed of *genes*, can be used to represent each individual from the perspective of genetic. A *gene fragment* refers to several continuous genes within one chromosome, which corresponds to specific arrangement of some adjacent atoms in the NP. The well-known GA operations, such as *selection*, *crossover* and *mutation*, are performed over specific gene fragment. During the evolution, the present generation can be called as *parents*, while the next generation can be called as *children*.

Step 1: Initializing the population. Initializing the population is the first step to start the whole GA process and only runs once. It consists of two stages. The first stage is to arrange all the atomic coordinates in the NP, which are derived from the corresponding model, as described in Section 2.1. Assuming that the total number of atoms in the NP is N, where the number of Pd atoms and Ag atoms is N_1 and N_2, then the NP can be represented by a list of N atomic coordinates (x_i, y_i, z_i). As to the order of these coordinates, there is no restriction. However, once determined, it will remain unchanged during the whole GA process. The second stage is to randomly initialize a population of several individuals. What should be mentioned, although the atomic arrangements of each individual in the population are different from each other, the atomic coordinates are the same.

Step 2: Calculating the total energies. The second step is to calculate the total energy of each NP in the population using molecular statics simulations. The population can be either initialized in *Step 1* or generated by GA loop in *Step 6*. The computational details of molecular statics simulations will be given in Section 2.3. The calculated energies can be used to evaluate the fitness values of corresponding NPs, as described in *Step 4*.

Step 3: Coding the population. To facilitate the subsequent GA procedures, each individual in the population should be coded into a binary string according to the atomic arrangement of the NP. In present work, Pd atom is encoded as 1 and Ag atom is encoded as 0. Then each NP can be represented by a binary string of length N, the number of 1 and 0 in which is N_1 and N_2, as shown in Fig. 2(b). For NPs with different atomic arrangements, the corresponding binary strings are different.

Step 4: Calculating the fitness values. To save the best individuals in each generation, the fitness value of each individual should be calculated. Generally, the fitness value should be able to reflect the competitiveness of the corresponding individual in the generation. That's to say, the fitness values should be larger for more competitive individuals and lower for weaker ones. In present work, the fitness value is calculated using the following equation:

$$\mathrm{F} = \exp\left[-p\left(\frac{E - E_{\min}}{E_{\max} - E_{\min}}\right)\right],$$

where E is the total energy of corresponding NP, which can be obtained in *Step 2*; $E_{\min}$ and $E_{\max}$ denote the minimum and maximum energies in the generation, respectively; p is scaling factor and set to -3 according to experience in present work. (Effects of the scaling factor on the optimization process are given in Supplementary Information.)

Step 5: Saving the elites. In classical GA, the GA operations (such as selection, crossover and mutation) are performed over all individuals in the parents' generation, which may result in the decline of the population, especially for near-optimal population. To avoid the decline and enhance the efficiency of the optimization process, the classical GA is modified by adding present step. Specifically, a certain number of individuals with larger fitness values in the population, as the so-called *elites*, are chosen and directly saved from the parents' generation to the children's generation without any subsequent GA operations, as shown in Fig. 2(c). This step can guarantee that the best individuals in parents' generation, corresponding to the NPs with the lowest energies, can be passed to the children's generation successfully.

Step 6: GA loop. GA loop is the core operation of the whole GA process and is used to generate new individuals of the children's generation. Generally, three stages, as selection, crossover and mutation, are included in each GA loop iteration, as shown in Fig. 2(d).

The first stage is ***selection*** and the most common algorithm is Roulette wheel selection, which is also used in present work. Specifically, the probability of each individual being selected equals to the corresponding fitness value divided by the sum of all fitness values in the population. Apparently, the sum of all probabilities in the population equals to 1. A random number between 0 and 1 is generated to select one individual from the population. Using such scheme, individuals with larger fitness values are more likely to be selected. Despite that, those with lower fitness values still keep the possibility of being selected. To facilitate the following *crossover* stage, two individuals are selected using the same scheme independently.

The second stage is ***crossover***, which has the most significant impact on the next generation. Fig. 2(d) illustrates the crossover operation schematically. The two individuals selected in the above *selection* stage are regarded as the parents' chromosomes. Then two gene fragments, starting from the same position and having the same length, are selected randomly from the two individuals. If the two fragments are not exactly the same and have the same number of 1 or 0, they are exchanged to generate two new individuals; if the two gene fragments are the same or have a different number of 1 or 0, two new fragments will be selected using the *selection* operation until the conditions of exchange are met and the exchange is completed. The reason why the same number of 1 or 0 in the gene fragments is required is to guarantee that the number of Pd or Ag atoms in the final NP remains unchanged.

The third stage is ***mutation***, which can help to improve the diversity of the next generation. As shown in Fig. 2(d), two single genes are selected randomly from one individual firstly. If the two genes are not the same, they are exchanged directly to generate a new individual; if not, two new genes will be selected until the condition of exchange is met and the exchange is completed. The *mutation* operation is performed over the two new individuals obtained in the above *crossover* stage. As a result, two newer individuals will be obtained.

For one GA loop, two individuals in the children's generation can be obtained. To keep the whole GA process going, the number of individuals in the children's generation should be the same as that in the parents' generation. Hence, the GA loop needs to be performed for many times. It should be noted that several individuals of the children's generation have been obtained by saving the elites in *Step 5*, so only a part of individuals need to be generated by means of GA loop. After the GA loop step, a newer and better population can be obtained.

Step 7: Termination. Termination is the final step, which is used to determine whether the optimization process should be stopped. In

Table 1
Calculated physical properties of Pd and Ag using EAM potential, with available experimental data as a comparison. The experimental lattice constants and cohesive energies are taken from literature [23]. The experimental surface energies are from literature [24].

	Lattice constant (Å)		Cohesive energy (eV)		Surface energy (erg/cm^2)			
	Expt.	EAM	Expt.	EAM	E_{poly}	$E_{(100)}$	$E_{(110)}$	$E_{(111)}$
Pd	3.89	3.89	−3.89	−3.91	2043	1648	1839	1510
Ag	4.09	4.09	−2.95	−2.85	1320	763	863	750

present work, the number of iterations is used as the criterion: if the number of iterations is larger than a pre-defined number, the optimization process will be stopped and the newest population will be output as the optimal one; if not, the above *Step 2* to *Step 6* will be repeated, starting with the new population obtained in *Step 6*. As to the pre-defined number, it is determined empirically.

2.3. Molecular simulations

During the optimization process using the improved genetic algorithm, molecular statics simulations, which are implemented by LAMMPS [18], are used to calculate the total energy of each NP in present work. In the simulations, embedded atom method (EAM) potential, which was developed by Zhou et al. [19,20] and widely applied to a large number of related researches including surfaces [21] and nanoparticles [22], is used to describe the interactions of Pd-Ag system. To verify the potential, some basic physical properties of Pd and Ag, including the equilibrium lattice constant, cohesive energy and the surface energies of three low-index facets (1 0 0), (1 1 0), (1 1 1), are calculated and compared with available experimental data, as listed in Table 1. From the table, it can be seen that the calculated lattice constants and cohesive energies agree very well with corresponding experimental data. Regarding the surface energies, the experimental data is extrapolated values for individual polycrystalline solids. By comparison, it can be noted that the calculated surface energies are in the same level as the corresponding experimental values. Hence, the EAM potential used in present work has a relatively high precision in describing the Pd-Ag system.

To explore the melting behavior of Pd-Ag NPs, MD simulations are performed. For each shape, four NPs with the same Ag concentration of 0.5 and different sizes from 2.5 nm to 5.0 nm are studied. In all simulations, periodic boundary condition is employed. To avoid interactions between the original NP and adjacent mirrors, the simulation box is set large enough to exceed the range of atomic interactions. To simulate the melting process of NPs, canonical ensemble is adopted and the temperature is raised from 100 K to 2000 K with an interval of 100 K. The time step is set to 2 fs. For each calculation, 50 ps is spent to reach the thermodynamic equilibrium state, and then statistical data is gathered over 150 ps.

To characterize the melting point of NPs, *Lindemann index* is adopted as the indicator [25,26]. The definition of Lindemann index can be given as:

$$\delta = \frac{2}{N(N-1)} \sum_{i<j} \frac{\sqrt{\langle r_{ij}^2 \rangle_t - \langle r_{ij} \rangle_t^2}}{\langle r_{ij} \rangle_t},$$

where r_{ij} is the distance between the i-th atom and the j-th atom, N is the number of atoms in the NP, $\diamond_t$ denotes the time average over referred physical quantity.

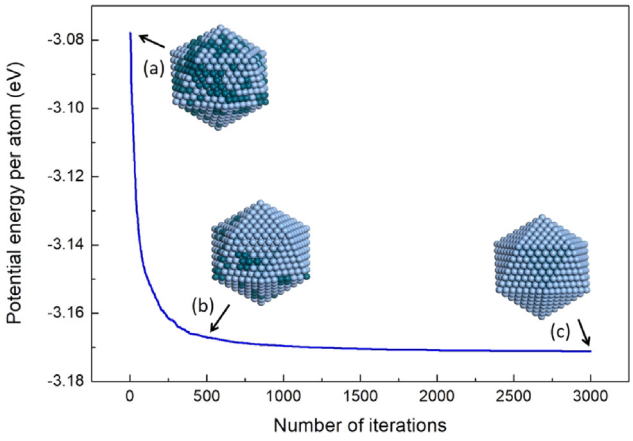

Fig. 3. Potential energy per atom as a function of iteration numbers for one specified Pd-Ag NP (icosahedral shape, a total of 1415 atoms, Ag concentration of 0.5); Pd atoms and Ag atoms are denoted by mazarine and French grey, respectively. Inserted pictures: (a) Initial configuration; (b) Intermediate configuration at 500th step; (c) Final configuration at 3000th step.

3. Results and discussions

3.1. Model optimization

To illustrate the effectiveness of the improved genetic algorithm, the evolutionary curve of the potential energy per atom as a function of iteration number is drawn for one specified Pd-Ag NP (icosahedral shape, a total of 1415 atoms, Ag concentration of 0.5), as shown in Fig. 3. It can be seen that the potential energy per atom is relatively high at the initial stage, which is due to the disordered atomic arrangement as a result of random generation, as shown in Fig. 3(a). With the number of iterations increasing, the potential energy per atom decreases rapidly. At almost 500th step, the potential energy has already been relatively low. Fig. 3(b) shows the corresponding atomic arrangement, which is quite orderly. Meanwhile, the Ag atoms tend to aggregate in the surface. After that, although the potential energy continues to decrease, the magnitude is very limited. After 2000th steps, the potential energy remains essentially unchanged, which denotes that the corresponding structure has already been energetically stable. Fig. 3(c) shows the final optimized atomic arrangement of the Pd-Ag NP at 3000th steps. It can be found that Ag atoms occupy all the surface positions and all Pd atoms are encapsulated inside the NP.

Using similar approach, the atomic arrangement of all involved Pd-Ag NPs with different shapes, different compositions and similar sizes can be optimized. The corresponding results are listed in Fig. 4. In details, the eight shapes introduced in Section 2.1 are considered. For each shape, three different concentrations of Ag are investigated, as 0.2, 0.5 and 0.8. Regarding the size, it is impossible to make the NPs with different shapes have the same number of atoms. Despite that, similar number of atoms is guaranteed for all the involved NPs, from a minimum of 1288 for TD shape to a maximum of 1481 for SP shape. To clearly show the atomic arrangement in the center, the cross-section view of each NP is given aside the main view. The detailed number of atoms and concentration of Ag are listed below each two sub-figures.

For all Pd-Ag NPs listed in Fig. 4, the first conclusion that can be easily drawn is that Ag atoms tend to occupy the surface positions, while Pd atoms prefer to occupy the central positions. Such a conclusion is reasonable. From Table 1, the surface energies of Ag atoms are much lower than those of Pd atoms, so the total energy can be lower and the corresponding NP can be more stable if more Ag atoms occupy the surface positions. When the concentration of Ag is 0.2, all Ag atoms appear only on the surface positions for all NPs. For all NPs except the TH-shaped one, Ag atoms are not enough to cover all the surface positions, they prefer to occupy the corner positions and edge positions.

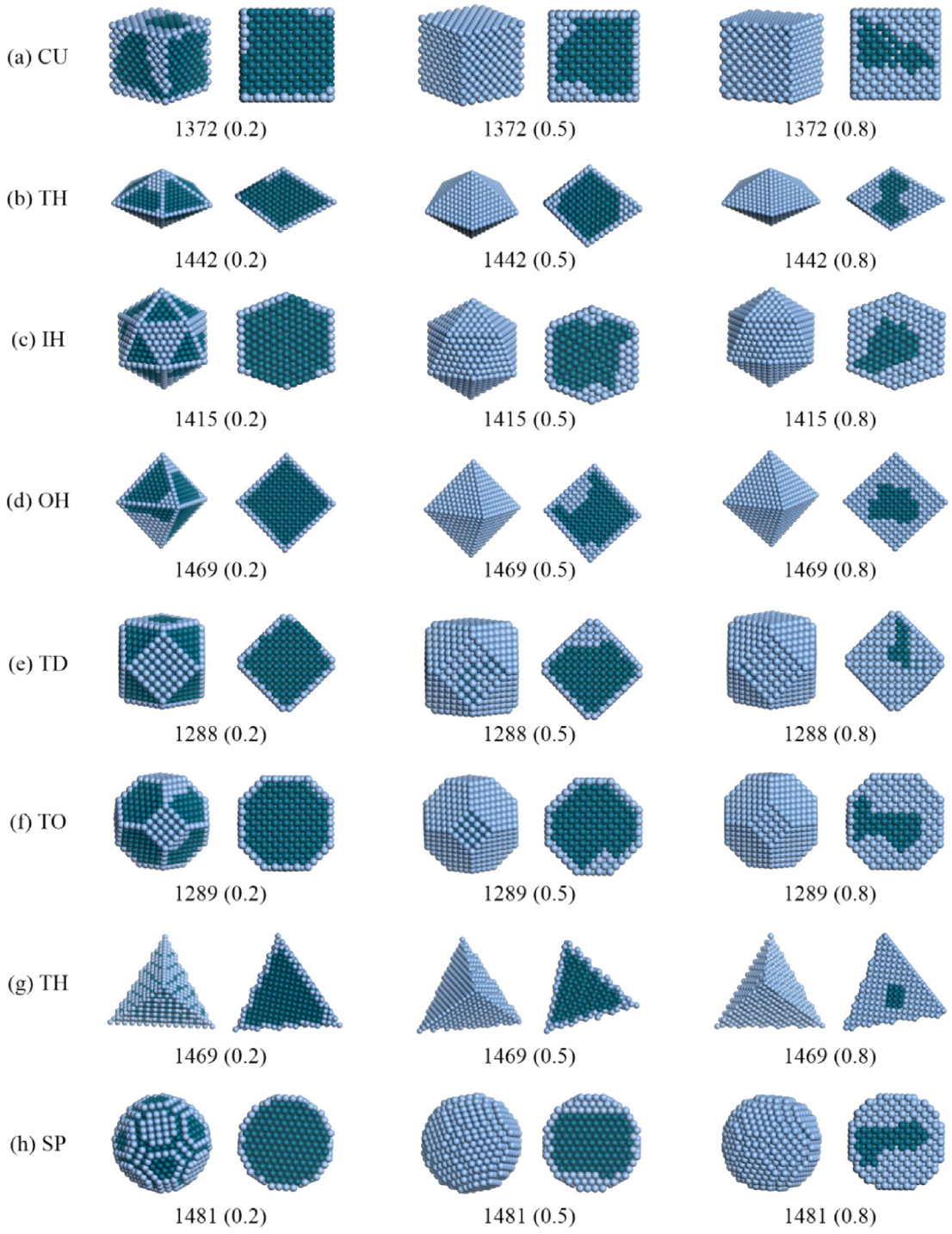

Fig. 4. Optimized atomic arrangement of Pd-Ag NPs with eight shapes and three concentrations of Ag. For each two columns of one NP, the left is the main view and the right is the cross-section view. For each row, the shapes are the same, while the concentrations of Ag are different, as 0.2, 0.5, 0.8 from left to right. Pd atoms are in mazarine and Ag atoms are in french grey.

As the concentration of Ag increases to 0.5 or 0.8, all surface positions are occupied by Ag atoms and all Pd atoms are encapsulated inside the NPs. Meanwhile, it can be seen that the Pd atoms in the core tend to aggregate together instead of being separated by Ag atoms. This can be attributed to the stronger interaction between two Pd atoms than that between Pd atom and Ag atom. What should be mentioned, although both Pd and Ag tend to aggregate in NPs from the perspective of energetics, it is possible for their mixing in experiments. In fact, it has been proved that Pd and Ag can be mixed in both bulk and nanostructures and form miscible solid solutions [12,27]. The main reason for such inconsistency is that the optimization algorithm employed in present work can only give the optimal configurations from the perspective of energetics, without considering the influence of many practical factors, such as temperature, chemical environment and so on, which may play significant roles in experiments.

3.2. Structural stability

The structural stability plays a significant role for the application of bimetallic NPs. In present work, the structural stability of Pd-Ag NPs

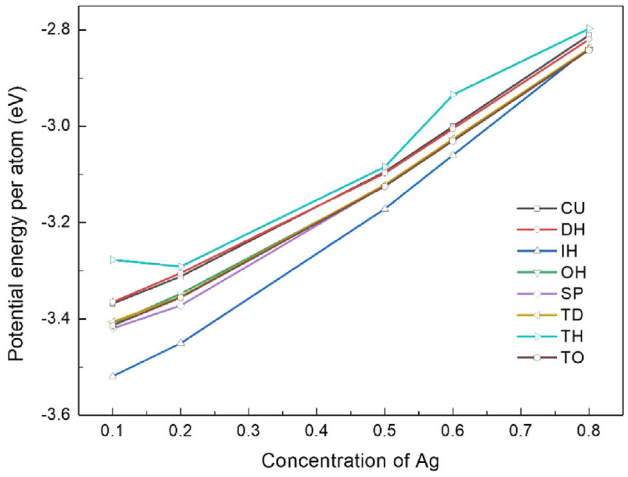

Fig. 5. Potential energy per atom as a function of Ag concentration for Pd-Ag NPs with different shapes and similar size.

with different shapes, compositions and sizes are studied systematically from the view of energetics.

Firstly, the curve of potential energy per atom changing with the Ag concentration of Pd-Ag NP for each shape is drawn in Fig. 5. The NPs involved here are similar in size. It can be seen that the potential energy per atom increases with the concentration of Ag for all involved NPs. Such tendency can be explained from the perspective of cohesive energy. From Table 1, the cohesive energy of Ag is larger than that of Pd, so the increase of Ag atoms can lead to the increase of the overall potential energy. By comparing the potential energy of NPs with the same Ag concentration and different shapes, it can be found that the IH-shaped NPs have the lowest energies, while the TH-shaped ones have the highest energies. Considering that the number of atoms is very close for these NPs, the magnitude of potential energy can basically represent the structural stability of corresponding NP. Hence, it can be concluded that the Pd-Ag NPs with IH shape are the most stable, while those with TH shape are the least stable.

To learn about the effect of particle size on the structural stability of Pd-Ag NP, the curve of potential energy per atom as a function of particle size for each shape is drawn in Fig. 6. The concentration of Ag for all involved NPs here is 0.5. The particle sizes are between 2.5 nm and 5.2 nm and with slight difference for different shapes. From the figure, the potential energy decreases with the increase of particle size. From the view of energetic, the atoms with lower coordination numbers have higher potential energy. For small-sized NPs, the proportion of surface atoms, which are atoms with low coordination numbers, is relatively high and therefore the corresponding potential energies are relatively high. By comparing the positional relationship of these curves, it can be found that the potential energy curves of the eight different shaped NPs satisfies the following rule: IH < TD < CU/TO < SP < OH < DH < TH. The NPs with IH shape have the lowest energies, while those with TH shape have the highest energies. Hence, the same conclusion can be drawn that IH-shaped NPs are the most stable and TH-shaped ones are the least.

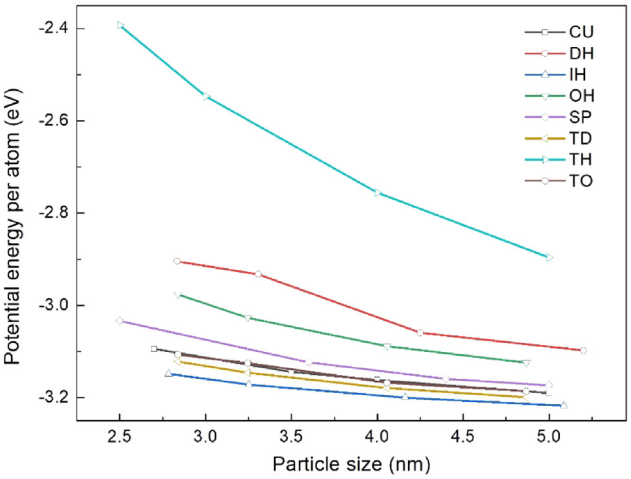

Fig. 6. Potential energy per atom as a function of particle size for Pd-Ag NPs with eight different shapes and same Ag concentration of 0.5.

3.3. Melting behavior

Furthermore, the melting behavior of Pd-Au NPs are studied using MD simulations. To illustrate the method used during the study, IH-shaped Pd-Ag NP, which has been proven to be the most stable in previous simulations, is chosen as an example. Five IH-shaped Pd-Ag NPs with the same Ag concentration of 0.5 and different sizes (which are 1.39 nm, 2.78 nm, 3.25 nm, 4.16 nm and 5.09 nm, respectively) are constructed. Then MD simulations are performed over each NP. After that, Lindemann index, which is used to characterize the structural evolution of NP during the heating process, is calculated for each NP. Fig. 7 draws the Lindemann index as a function of temperature for all the five involved Pd-Ag NPs. It can be seen clearly that there are three distinct regions for each curve. When the temperature is relatively low, Lindemann index increases slowly with the temperature. When the temperature reaches a certain value, Lindemann index increases sharply within a narrow temperature range. Then the index continues to increase gradually but at a slope larger than that at the first stage. According to the characteristics of the curves, the temperature corresponds to the sharp increase can be defined as the melting point of the corresponding NP. From the figure, it can be found that the melting point of the IH-shaped nanoparticles increases with the particle size.

Using the same method, the curves of melting point changing with particle size for Pd-Ag NPs with the same Ag concentration of 0.5 and different shapes are calculated and drawn in Fig. 8. It can be seen that the melting points are different for Pd-Ag NPs with different shapes or sizes. In other words, the melting point of Pd-Ag NPs is both shape-dependent and size-dependent, which is quite different from bulk materials. For different shaped NPs, the NPs with TH shape have the lowest melting points, while those with IH shape have the highest melting points. By comparing the positional relationship of these curves, the melting points of the eight different shaped NPs satisfy the following relationship: IH > TD/CU > TO > SP > OH > DH > TH. It can

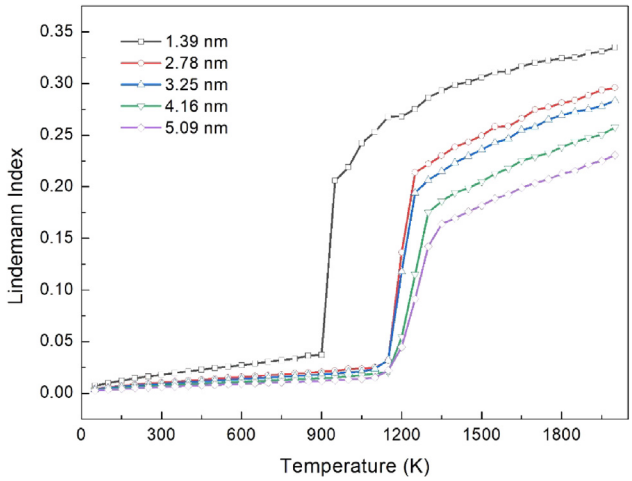

Fig. 7. Lindemann index as a function of temperature for five IH-shaped Pd-Ag NPs with the same Ag concentration of 0.5 and different particle sizes from 1.39 nm to 5.09 nm.

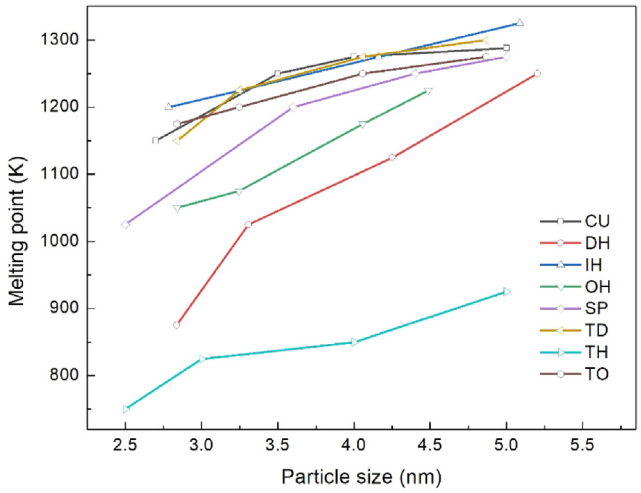

Fig. 8. Melting point as a function of particle size for Pd-Ag NPs with the same Ag concentration of 0.5 and eight different shapes and.

be found that such relationship chain is just the opposite of the previously obtained one for potential energy per atom. Hence, it can be concluded that a more stable Pd-Ag NP from the view of energetics generally has a higher melting point. The relationship between structural stability and melting point of NP can be explained from the perspective of atomic activity. For less stable NPs, the atomic activity is higher and the corresponding ability of atomic diffusion and migration is also stronger, which to some extent promotes the melting of NPs. For experimental Pd-Ag NPs, since they are not necessarily the most stable from the perspective of energetics and the configurational entropy might be higher, the corresponding melting points would be lower than those presented in this work.

4. Conclusion

In present work, Pd-Ag bimetallic NPs with eight typical shapes and three compositions are optimized using improved genetic algorithm accompanied by molecular statics simulations. The structural stability of Pd-Ag NPs with different shapes, compositions and sizes is studied from the view of energetics. It is found that Pd-Ag NPs with icosahedral shape are the most stable and those with tetrahedral shape are the least stable. Moreover, the melting behavior of Pd-Ag NPs is explored by performing MD simulations. Lindemann index is employed as the indicator of melting point. It is concluded that the melting point of Pd-Ag NPs is both shape-dependent and size-dependent. Specifically, Pd-Ag NPs with icosahedral shape have the highest melting points and those with tetrahedral shape have the lowest melting point. Besides, the relationship between structural stability and melting points of Pd-Ag NPs has also been revealed. The conclusions obtained in present work can provide guidance for experimental designs of Pd-Ag NPs.

CRediT authorship contribution statement

Mingming Guo: Data curation, Formal analysis, Investigation, Software. **Huizhen He:** Visualization. **Zhipeng Zhang:** Investigation. **Zhitian Liu:** Supervision. **Feng Xie:** Funding acquisition. **Bin Shan:** Conceptualization, Supervision, Writing - review & editing. **Xianbao Duan:** Funding acquisition, Conceptualization, Methodology, Supervision, Validation, Writing - review & editing.

Declaration of Competing Interest

The authors declare that they have no known competing financial interests or personal relationships that could have appeared to influence the work reported in this paper.

Acknowledgements

This work is supported by the National Natural Science Foundation of China (11604247), Youths Science Foundation of Wuhan Institute of Technology (k201628) and Key Laboratory of Advanced Reactor Engineering and Safety, Ministry of Education (No. ARES-2018-04).

Appendix A. Supplementary data

Supplementary data to this article can be found online at https://doi.org/10.1016/j.commatsci.2020.109520.

References

[1] D.L. Fedlheim, C.A. Foss, Metal Nanoparticles: Synthesis, Characterization, and Applications, CRC Press, 2001.
[2] C.N.R. Rao, A. Müller, A.K. Cheetham, The Chemistry of Nanomaterials: Synthesis, Properties and Applications, John Wiley & Sons, 2006.
[3] I. Khan, K. Saeed, I. Khan, Arab. J. Chem. (2017).
[4] A. Zaleska-Medynska, M. Marchelek, M. Diak, E. Grabowska, Adv. Colloid Interface 229 (2016) 80.
[5] X. Liu, D. Wang, Y. Li, Nano Today 7 (2012) 448.
[6] K.S. Ranjith, A. Celebioglu, T. Uyar, Nanotechnology 29 (2018) 245602.
[7] D. Bochicchio, R. Ferrando, R. Novakovic, E. Panizona, G. Rossi, Phys. Chem. Chem. Phys. 16 (2014) 26478.
[8] F. Lu, D. Sun, J. Huang, M. Du, F. Yang, H. Chen, Y. Hong, Q. Li, ACS Sustain Chem. Eng. 2 (2014) 1212.
[9] N.A. Khan, S. Shaikhutdinov, H.J. Freund, Catal. Lett. 108 (2006) 159.
[10] B. Sharma, J.S. Kim, Int. J. Hydrogen Energy 43 (2018) 11397.
[11] S.K. Sengar, B.R. Mehta, Govind, J. Appl. Phys. 112 (2012) 014307.
[12] D. Lahiri, B. Bunker, B. Mishra, Z. Zhang, D. Meisel, C.M. Doudna, M.F. Bertino, F.D. Blum, A.T. Tokuhiro, S. Chattopadhyay, T. Shibata, J. Terry, J. Appl. Phys. 97 (2005) 094304.
[13] S.Q. Wu, M. Ji, C.Z. Wang, M.C. Nguyen, X. Zhao, K. Umemoto, R.M. Wentzcovitch, K.M. Ho, J. Phys.: Condens. Matter 26 (2013) 035402.
[14] G.F. Shao, T.N. Wang, T.D. Liu, J.R. Chen, J.W. Zheng, Y.H. Wen, Comput. Phys. Commun. 186 (2015) 11.
[15] G.F. Shao, N.N. Tu, T.D. Liu, L.Y. Xu, Y.H. Wen, Physica E 70 (2015) 11.
[16] X. Duan, B. He, M. Guo, Z. Liu, Y. Wen, B. Shan, Comput. Mater. Sci. 150 (2018) 418.
[17] X. Duan, F. Xie, X. Guo, Z. Liu, J. Yang, X. Liu, B. Shan, Comput. Mater. Sci. 156 (2019) 268.
[18] S. Plimpton, J. Comput. Phys. 117 (1995) 1.
[19] M.S. Daw, M.I. Baskes, Phys. Rev. B 29 (1984) 6443.
[20] X.W. Zhou, R.A. Johnson, H.N.G. Wadley, Phys. Rev. B 69 (2004) 144113.
[21] S. Verma, T. Rehman, A. Chatterjee, Surf. Sci. 613 (2013) 114–125.
[22] S.J. Guo, X. Zhang, W.L. Zhu, K. He, D. Su, A. Mendoza-Garcia, S.F. Ho, G. Lu, S.H. Sun, J. Am. Chem. Soc. 136 (2014) 15026.
[23] C. Kittel, Introduction to Solid State Physics Vol. 8 Wiley, New York, 1976.
[24] B.-J. Lee, J.-H. Shim, M.I. Baskes, Phys. Rev. B 68 (2003) 144112.
[25] F.A. Lindemann, Phys. Z. 11 (1910).
[26] S. Alavi, D.L. Thompson, J. Phys. Chem. A 110 (2006) 1518.
[27] V. Ruiz-Ruiz, R. González-Olvera, R. Díaz-Pardo, I. Betancourt, I. Zumeta-Dubé, D. Díaz, N. Farfán, M.J. Arellano-Jiménez, Materialia 4 (2018) 166–174.